

MedChemComm

Accepted Manuscript



This is an *Accepted Manuscript*, which has been through the Royal Society of Chemistry peer review process and has been accepted for publication.

Accepted Manuscripts are published online shortly after acceptance, before technical editing, formatting and proof reading. Using this free service, authors can make their results available to the community, in citable form, before we publish the edited article. We will replace this *Accepted Manuscript* with the edited and formatted *Advance Article* as soon as it is available.

You can find more information about *Accepted Manuscripts* in the [Information for Authors](#).

Please note that technical editing may introduce minor changes to the text and/or graphics, which may alter content. The journal's standard [Terms & Conditions](#) and the [Ethical guidelines](#) still apply. In no event shall the Royal Society of Chemistry be held responsible for any errors or omissions in this *Accepted Manuscript* or any consequences arising from the use of any information it contains.

ARTICLE

Synthesis, biological evaluation and QSAR studies of diarylpentanoid analogues as potential nitric oxide inhibitors

Cite this: DOI: 10.1039/x0xx00000x

Received 00th January 2012,
Accepted 00th January 2012

DOI: 10.1039/x0xx00000x

www.rsc.org/

S. M. Mohd Faudzi^{a,b}, S. W. Leong^a, F. Abas^{*a,c}, M. F. F. Mohd Aluwi^d, K. Rullah^d, K. W. Lam^d, S. Ahmad^e, C. L. Tham^f, K. Shaari^{a,b}, and N. H. Lajis^{*a}

A series of forty-five 1,5-diphenylpenta-2,4-dien-1-one analogues were synthesized and evaluated for their nitric oxide (NO)-inhibition activity in IFN- γ /LPS-activated RAW 264.7 cells. Compounds **3h**, **7a**, **7d** and **7e** exhibited comparable or significantly higher activity as compared to the standard, curcumin ($IC_{50}=14.69\pm 0.24$ μ M). Compound **7d**, a 5-methylthiophenyl-bearing analogue, displayed the most promising NO-inhibitory activity with an IC_{50} value of 10.24 ± 0.62 μ M. The 2D and 3D QSAR analyses performed revealed that a *para*-hydroxyl group on ring B and an α,β -unsaturated ketone moiety on a linker are crucial for remarkable anti-inflammatory activity. Based on ADMET and TOPKAT analyses, compounds **3h**, **7a** and **7d** are predicted to be nonmutagenic and to exhibit high blood–brain barrier (BBB) penetration, which indicates that they are potentially effective drug candidates for the treating central nervous system (CNS) related disorders.

Introduction

Inflammation is a complex component of an animal's response system in response to a variety of stimuli resulting from biological, chemical, and physical invasions or damages. However, prolonged exposure to a stimulus can lead to a chronic phase. It has been reported that chronic inflammation may lead to the development of numerous diseases, including cancer,¹ chronic asthma, cardiovascular diseases, diabetes, autoimmune diseases, atherosclerosis, allergies, rheumatoid arthritis, bowel inflammation, psoriasis, multiple sclerosis, and accelerated aging.²

NO is a short-lived bioactive free radical synthesized from L-arginine, NADPH and molecular oxygen by the catalytic reaction of nitric oxide synthase (NOS), which has an important function as an intercellular messenger in the regulation of physiological and pathophysiological mechanism in the nervous, cardiovascular and immunological systems.^{3,4} Excessive generation of NO enhances the production of diverse inflammatory mediators and may contribute to the immunopathology of macrophage-dependent inflammation⁵ and degenerative diseases, including cancer and cardiovascular disorders. Therefore, an inhibitory effect on NO production is a promising therapeutic target for potential anti-inflammatory agents. It is well-documented that inducible nitric oxide synthase (iNOS) is expressed in response to various stimuli (LPS, IFN- γ or TNF- α), which causes the production of a vast amount of NO by macrophages during the inflammatory process,⁶ while the expression of several pro-inflammatory mediators, such as NO, is regulated at the transcriptional level by nuclear factor- κ B (NF- κ B).⁷

Diarylpropanoids (such as flavonones and chalcones), diarylheptanones (especially curcumins and their derivatives) and divinylketonoids (such as zerumbone) are natural products commonly found in Zingiberaceae plants, especially *Curcuma domestica*, *Alpinia rafflesiana*, and *Zingiber zerumbet*, respectively.^{8,9} These compounds have been shown to display excellent anti-inflammatory activity through their actions on a number of mediators and promoters.¹⁰ Curcumin (Fig. 1) has been one of the most investigated diarylheptanoids due to its strong bioactivity, but its instability under physiological conditions, poor absorbability and fast metabolism have limited its potential practical use.¹¹ A number of studies have shown that a diarylpentadienone scaffold enabled their anti-inflammatory properties via NO-production suppression activity and the inhibition on proinflammatory cytokines such as TNF- α and IL-6.^{12,13} Previously, we synthesized a series of diarylpentanoid monocarbonyl analogues¹³ (Fig. 1), and they were observed to enhance the stability *in vitro* and improve the pharmacokinetic profiles, particularly those related to anti-inflammatory activity.¹³⁻¹⁵

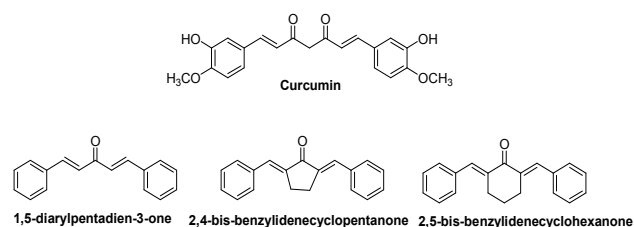


Fig. 1 Curcumin and its diarylpentanoid analogues

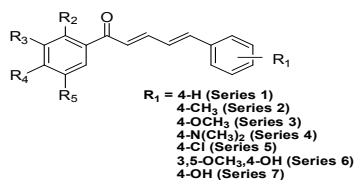
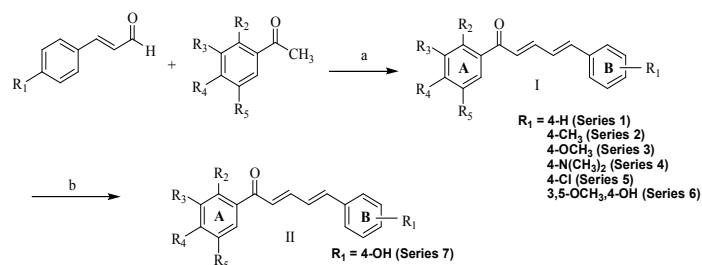


Fig. 2 Representative structure of 1,5-diphenylpenta-2,4-dien-1-one



Scheme 1 Reagents and conditions: (a) NaOH, ethanol, RT (overnight); (b) BBr₃, CH₂Cl₂ 0 °C (1h).

Continuing the interest in understanding the biological implications of the structural features in diarylpentanoids, we have prepared forty-five 1,5-diphenylpenta-2,4-dien-1-one analogues (Fig. 2). Unlike the commonly studied diarylpentanoid and curcumin series reported earlier, in which the carbonyl is located at the middle carbon,^{13,16} the ketone functionality in the new series is located at C-1 of the pentadienone linker moiety. It would be expected that the electronic character of the carbonyl, which may contribute in the ligand-receptor interaction, may be somewhat influenced by its position of being directly attached to one of the two aromatic rings. Herewith, we describe the synthesis of all of the analogues and the evaluation of their NO-suppression activity on IFN- γ /LPS-activated RAW 264.7 cells. To explore the interaction and effects of the diarylpentadienone analogues on the inflammatory mediator, we performed 2D and 3D QSAR analysis. It is hoped that further understanding may be gained through the correlations established between the physicochemical features, electronics and steric factors and the biological potency.

Results and discussion

Chemistry

1,5-Diarylpenta-2,4-dien-1-one analogues **I** (Series 1-6) were synthesized via Claisen-Schmidt condensation by reacting the appropriate cinnamaldehyde and substituted acetophenone in ethanolic sodium hydroxide for 24 h (see Scheme 1). The presence of an electron-donating group at the *para* position in the acetophenones (origin of ring B) appeared to improve the yield up to 90%. Conversely, lower yields in the range of 13 to 65% were obtained when an electron-withdrawing group was present in the aromatic ring of the cinnamaldehyde. This trend correlates well with the results of a previous study on the preparation of flavanones from 2'-hydroxychalcone.¹⁷ The cyclization of a chalcone containing an electron-donating group afforded a high yield, whereas the presence of electron-withdrawing and bulky groups resulted in lower product yields. The use of five-

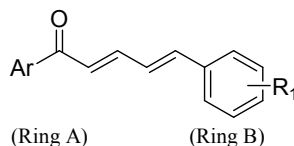
membered heterocyclic analogues of an acetophenone yielded the respective products in the range of 15 to 90%. It is noteworthy that the 5-methyl-thiophenyl-containing analogues gave better yields (greater than 70%).

The resulting methoxylated diarylpentadienones were then further demethylated to their polyphenolic analogues **II** (Series 7), using boron tribromide in dichloromethane (see Scheme 1), with the yields ranging from 20 to 75%. All of the purified diarylpentadienone analogues were characterized via ¹H- and ¹³C-nuclear magnetic resonance (NMR) as well as mass spectrometry. Based on the NMR data, the coupling-constant (*J*) values of the double bond of the two methylene units in the pentadiene chain are in the range of 7-8 Hz, indicating that the compounds are in the *cis* configuration.

NO inhibition in LPS/IFN- γ -induced macrophages

The inhibitory potency of the 1,5-diphenylpenta-2,4-dien-1-one analogues on LPS/IFN- γ -stimulated inflammation was first investigated in RAW 264.7 macrophage cells at a 50 μ M concentration. Based on the preliminary evaluation, twenty-five compounds were shown to significantly inhibit the LPS/IFN- γ -stimulated NO production, indicating that our diarylpentadienone scaffold may possess interesting anti-inflammatory property. The IC₅₀ values of the twenty-five bioactive compounds were determined and compared to that of the positive control, curcumin. In addition, MTT assays were performed to ensure that the nitric oxide inhibition in the RAW 264.7 cells was not due to cytotoxic activity. The efficacy of the 1,5-diphenylpenta-2,4-dien-1-one analogues on the nitrite production in the macrophage cells is shown in Table 1. The results of the NO-inhibitory screening showed that compounds **3h**, **7a**, **7d** and **7e** displayed potent anti-inflammatory activity with IC₅₀ values of less than 20 μ M. Additionally, seven other compounds (**1c**, **3i-k**, **3q**, and **7b-c**) significantly inhibited NO production, with IC₅₀ ranged between 20.0-30.0 μ M.

In series 1 of diarylpentadienone analogues, the most significant NO suppression effect is exhibited by compound **1c**, which contains a *meta*-hydroxylated phenyl ring. In contrast with compound **1b**, an *ortho*-hydroxyl bearing analogue did not contribute towards the activity enhancement. This observation can be best explain by the presence of chelated system in compound **1b**, in comparison to the absence such system in compound **1c**. This trend was further supported by a *meta*-hydroxylated on ring A as displayed by analogue **3h**, with the highest inhibition potency with the IC₅₀ of 16.3 μ M. Further comparisons of the variation of ring A in series 3, revealed three *para*-hydroxyl-bearing compounds, **3i-k** also showed a remarkable anti-inflammation property. Based on this result, it is interesting to note that a hydroxyl group on either *meta*- or *para*-position of ring A indicated the importance of this feature in the enhancement of NO inhibition activity as exhibited by compounds **3h-k**, as opposed the activity observed in the unsubstituted ring A such as compound **3a**. This finding correlated well with previous study,¹⁸ which suggested that the presence of hydroxyl group at *meta*- and/or *para*-position. The presence of these functionalities might contribute to higher electron density as well as higher hydrogen bond potential of the phenyl moiety, which could be participate in the π - π interaction or hydrogen bonding in the active site, that is important in the NO inhibitory activity.

Table 1. NO inhibitory activity and cytotoxicity of 1,5-diphenylpenta-2,4-dien-1-one analogues on RAW 264.

Compounds	R ₁ (Ring B)	Ar (Ring A)	NO inhibition (%) ± S.E.M at 50 μM	NO inhibition (μM) ± S.E.M	IC ₅₀	Cytotoxicity (μM) ± S.E.M	IC ₅₀
Curcumin	-	-	99.3 ± 0.2	14.7 ± 0.2	>100		
1a	4'-H	phenyl	66.8 ± 0.7	44.6 ± 2.5	44.3 ± 5.4		
1b	4'-H	2-hydroxyphenyl	<10	ND	ND		
1c	4'-H	3-hydroxyphenyl	103.9 ± 0.6	26.1 ± 0.1	48.7 ± 5.1		
1d	4'-H	4-methoxyphenyl	51.1 ± 4.8	71.2 ± 5.1	>100		
1e	4'-H	4-fluorophenyl	33.1 ± 4.2	ND	ND		
1f	4'-H	4-chlorophenyl	<10	ND	ND		
1g	4'-H	5-bromo-2-hydroxyphenyl	<10	ND	ND		
1h	4'-H	5-chloro-2-hydroxyphenyl	<10	ND	ND		
1i	4'-H	3,5-dichloro-2-hydroxyphenyl	19.6 ± 2.1	ND	ND		
1j	4'-H	5-methylthiophen-2-yl	52.6 ± 4.3	68.6 ± 2.6	>100		
1k	4'-H	2,5-dimethylfuran-3-yl	84.6 ± 1.1	59.0 ± 6.0	>100		
2a	4'-CH ₃	phenyl	73.7 ± 7.1	ND	ND		
3a	4'-OCH ₃	phenyl	77.4 ± 3.4	45.8 ± 1.5	>100		
3b	4'-OCH ₃	4-methoxyphenyl	41.6 ± 1.7	ND	ND		
3c	4'-OCH ₃	4-fluorophenyl	40.0 ± 3.3	ND	ND		
3d	4'-OCH ₃	5-chloro-2-hydroxyphenyl	26.4 ± 1.7	ND	ND		
3e	4'-OCH ₃	2,4-dimethoxyphenyl	<10	ND	ND		
3f	4'-OCH ₃	3,5-dichloro-2-hydroxyphenyl	<10	ND	ND		
3g	4'-OCH ₃	4-methylphenyl	42.2 ± 2.5	ND	ND		
3h	4'-OCH ₃	3-hydroxy-4-methoxyphenyl	100.2 ± 2.3	16.3 ± 2.0	28.4 ± 1.7		
3i	4'-OCH ₃	4-hydroxy-3,5-dimethoxyphenyl	89.4 ± 3.9	21.5 ± 2.3	58.6 ± 2.1		
3j	4'-OCH ₃	3-chloro-4-hydroxyphenyl	98.2 ± 0.9	23.5 ± 2.4	67.6 ± 5.0		
3k	4'-OCH ₃	2-fluoro-4-hydroxyphenyl	102.3 ± 1.6	21.8 ± 2.0	60.3 ± 5.4		
3l	4'-OCH ₃	5-methylthiophen-2-yl	41.7 ± 4.6	ND	ND		
3m	4'-OCH ₃	2,5-dimethylfuran-3-yl	59.7 ± 1.1	39.8 ± 2.3	>100		
3n	4'-OCH ₃	2,5-dimethylthiophen-3-yl	44.8 ± 5.2	ND	ND		
3o	4'-OCH ₃	1 <i>H</i> -pyrrol-2-yl	95.8 ± 1.7	57.4 ± 1.2	>100		
3p	4'-OCH ₃	thiophen-2-yl	69.6 ± 1.1	47.9 ± 5.5	68.5 ± 5.2		
3q	4'-OCH ₃	furan-2-yl	61.5 ± 2.4	27.5 ± 0.1	76.6 ± 3.7		
4a	4'-N(CH ₃) ₂	phenyl	51.2 ± 4.2	73.6 ± 7.5	>100		
4b	4'-N(CH ₃) ₂	4-methoxyphenyl	54.5 ± 1.3	77.4 ± 6.2	>100		
4c	4'-N(CH ₃) ₂	2-hydroxyphenyl	16.4 ± 3.1	ND	ND		
4d	4'-N(CH ₃) ₂	4-fluorophenyl	71.5 ± 4.8	63.8 ± 4.5	>100		
4e	4'-N(CH ₃) ₂	thiophen-2-yl	32.4 ± 2.8	ND	ND		
4f	4'-N(CH ₃) ₂	furan-2-yl	56.9 ± 3.5	115.9 ± 4.8	>100		
5a	4'-Cl	4-chlorophenyl	31.2 ± 4.0	ND	ND		
5b	4'-Cl	4-methoxyphenyl	45.4 ± 3.9	70.5 ± 2.1	80.2 ± 5.1		
5c	4'-Cl	5-chloro-2-hydroxyphenyl	<10	ND	ND		
6a	3',5'-OCH ₃ -4'-OH	phenyl	64.1 ± 5.0	42.0 ± 1.6	28.7 ± 4.1		
6b	3',5'-OCH ₃ -4'-OH	4-fluorophenyl	76.7 ± 1.1	39.3 ± 0.1	5.0 ± 3.6		
7a	4'-OH	4-hydroxyphenyl	101.8 ± 1.1	16.4 ± 0.3	>100		
7b	4'-OH	2,4-dihydroxyphenyl	82.1 ± 2.7	27.2 ± 1.1	>100		
7c	4'-OH	2-hydroxy-4-methoxyphenyl	93.4 ± 0.1	27.11 ± 0.7	>100		
7d	4'-OH	5-methylthiophen-2-yl	103.1 ± 1.6	10.2 ± 0.6	28.3 ± 2.9		
7e	4'-OH	4-fluorophenyl	110.2 ± 1.1	14.8 ± 1.9	45.49 ± 4.9		

ND = Not determined

The introduction of electron-withdrawing group on ring A regardless of their quantity and position does not lead to significant NO inhibitory activity, as displayed by compounds **1e-i** in comparison to its unsubstituted compound **1a**.

This observation suggested that low electron density of ring A was disfavour in enhancing the activity. A similar trend was also clearly demonstrated by the respective halogenated diarylpentadienone analogues, **3c**, **3d**, **3f**, **4d**, **5a**, **5c** and **6b**, whereby the presence of electron-withdrawing group in ring A was accompanied with

reduced inhibitory activity. This finding is consistent with the previous reports, which suggested that the introduction of halogen moiety in phenyl ring of chalcone¹⁹ and NSAIDs derivative U0126,²⁰ lowered the anti-inflammatory activity.

In contrast to the halogenated compounds previously mentioned with relatively poor activities, the analogues containing *para*-hydroxyl-bearing halogenated ring A such as compounds, **3j** and **3k** showed a significant NO inhibition property. This observation implied that the presence of 4-hydroxyl group in ring A may have veiled the negative impact of the electron-withdrawing group.

We also investigated the role of electron-donating group (methoxy and methyl) in ring A on the anti-inflammatory activity in series 1. The methoxylated compound **1d** was two-fold less active than the unsubstituted ring A analogue, **1a**, suggesting the high electron density is not important in improving NO inhibition. The same conclusion could also be drawn based on the reduced bioactivity displayed by analogues **3b**, **3e**, **3g**, **4b**, and **5b**. This was further supported by Manna et al,²¹ who showed that electron-releasing group (methoxy, methyl, di-methoxy) of 3-cyano-2(1H) pyridones resulted in weaker anti-inflammatory activity, possibly due to steric hindrance and/or lack of hydrogen bonding capability.²⁰

On the other hand, the replacement of phenyl group with heterocyclic scaffold, such as thiophenyl (**1j**) and furanyl (**1k**) in ring A resulted in mild NO inhibitory activity with IC₅₀ values of 68.6 μM and 59.0 μM, respectively. It is worth noting that furanyl exhibits a higher potential than thiophenyl ring due to its capability of forming hydrogen bond via its non-bonding electron pair, in comparison to sulphur species in which hydrogen bond formation is more susceptible towards aromatic π system, rather than with the unshared electron pair localized on S atom.²² Further variation in NO inhibition activity of heterocycle-containing analogues are exemplified by compounds **3l-q** and **4e-f**, where the furanyl-containing ring A (**3q**) exhibited the highest activity. This result were in close agreement with those of Qiu et al, which stated that thiophene-bearing 4-arylidene curcumin analogues demonstrated a reduction in activity in comparison to furanyl-bearing, indicating the S replacement of the O atom in heterocycle made a negative impact to its activity.²³

The strategy to demethylate the methoxy-bearing diarylpentadienone to form hydroxylated analogues had increased the bioactivity significantly, as displayed by analogues in series 7. The 5-methylthiophen-2-yl bearing analogue, compound **7d** recorded as the most potent NO inhibitor with IC₅₀ value of 10.7 μM. It is worth noting that the introduction of an electron-withdrawing (fluoro) and heterocyclic groups positively affects the NO inhibitory property in this series, in comparison to the respective analogues in series 1-6. This change in inhibitory activity may be rationalized by the crucial factor of the 4'-hydroxyl group in ring B, which mitigated the negative contributions of two groups mentioned above, resulting in the alteration of their interaction with the mediators.

Further structure-activity analyses of the variation in ring B were also performed to correlate the structural features with the NO inhibition activity. Among the diarylpentadienone analogues having phenyl group in ring A, all compounds composed of phenyl (**1a**), 4'-methylphenyl (**2a**), 4'-methoxyphenyl (**3a**), 4'-dimethylaminophenyl (**4a**) and 3,5-dimethoxy-4-hydroxyphenyl (**6a**) on ring B displayed mild to poor activity (see Table 1). Based on this result, it is possible to assume that difference in electron density on ring B did not significantly affected the inhibitory potency of compounds.

Among the 4-fluorophenyl containing analogues including **1e**, **3c**, **4d**, **6b** and **7e**, the highest inhibitory activity was displayed by analogue **7e**. This notable result illustrate that the presence of 4'-hydroxyl group on ring B, emerges to be a very important requirement for anti-inflammatory activity, as compound **7e** exhibited three fold better activity than compound **4d** (4'-dimethylamino substituted ring B) and two fold better inhibition than **6b** (3',5'-dimethoxy-4'-hydroxy substituted ring B). This trend may be explained by the fact that hydroxyl group can act as a stronger hydrogen bond acceptor than dimethylamino group in physiological pH environment. In this slightly basic condition, the hydroxyl group would form the negatively charged oxygen atom and possesses a stronger nucleophilic character, which in turn increases its tendency as hydrogen acceptor, in comparison to dimethylamino group. In addition, the bulky nature of 4'-dimethylamino and 3',5'-dimethoxy-4'-hydroxy may also contribute to its mild activity. On the other hand, the introduction of 4'-methoxy group in ring B (compound **3c**) did not improve the NO inhibitory activity. This must be due to its lower affinity for hydrogen bonding as compared to hydroxyl moiety.

The importance of 4'-hydroxyl group over 4'-methoxy and unsubstituted ring B could be clearly seen when ring A is composed of 5-methylthiophen-2-yl moiety. Compound **7d** exhibited six fold better NO inhibition activity than compound **1j**, a ring B unsubstituted 1,5-diphenylpenta-2,4-dien-1-one while compound **3l** displayed poor activity. These findings correlated well with the results of previous work in which a compound possessing an α,β-unsaturated ketone with 4'-hydroxylphenyl ring significantly suppressed the TNF-α-induced NF-κB activation.⁷ On the other hand, a significant role of 4'-methoxy over 4'-dimethylamino group on ring B in enhancing the NO inhibition has been proven by compounds **3p** and **3q** over compounds **4e** and **4f**, when ring A is composed of thiophenyl and furanyl rings. This could be clarified by the fact that the oxygen atom of the methoxy group has higher hydrogen bond accepting character as compared to the nitrogen atom of dimethylamino. Although the pK_a of dimethylamino group (pK_a ~10.61) is slightly higher than methoxy group (pK_a ~10.55), which confer its higher basicity with increasing hydrogen bond acceptor effect, the introduction of two methyl groups increases the steric bulk around the nitrogen atom. As the result water molecules are hindered from solvating the protonated form of dimethylamino compounds and prevents stabilization of this ion. This, in turn, decreases its hydrogen bond acceptor character of the respective compounds²⁴.

In summary, both rings (A and B) play a significant role in enhancing the anti-inflammatory activity in the diarylpentadien-1-one compounds. It is apparent that the presence of 4'-hydroxyl group on ring B (analogues of series 7) and either a 3-hydroxyl or 4-hydroxyl groups on ring A (such as compounds **1c** and **3h-k**) are the features that contribute to NO inhibitory activity.

Quantity structure-activity relationship (QSAR) analysis

2D QSAR

The 2D QSAR was performed to establish a consistent relationship between the biological activity of drugs and the effect of physicochemical and structural parameters on the chemical reactivity. The following equation shows the details of the optimal QSAR model generated by the GFA studies utilizing Discovery Studio 3.1, where r^2 is the correlation coefficient against 17 training compounds, r^2 (adj) is the r^2 adjusted value for the number of terms

in the model, and $r^2(\text{pred})$ is the predictive r^2 determined for the eight test compounds. Only linear terms were used for the development of the model, and pIC_{50} ($-\log \text{IC}_{50}$) was used as the dependent variable. The list of molecules involved and their calculated parameter values for the model are presented in Table 2.

Table 2. IC_{50} , pIC_{50} , number of rotatable bonds and MFPSA values of active compounds.

Compound	IC_{50}	pIC_{50}	Number of rotatable bond	MFPSA
1a	44.6 ± 2.5	4.351	4	0.072
1c	26.1 ± 0.1	4.583	4	0.15
1d	71.2 ± 5.1	4.148	5	0.098
1j	68.6 ± 2.6	4.164	4	0.18
1k	59.0 ± 6.0	4.23	4	0.115
3a	45.8 ± 1.5	4.339	5	0.098
3h	16.3 ± 2.0	4.787	6	0.178
3i	21.5 ± 2.3	4.669	6	0.167
3j	23.5 ± 2.4	4.63	5	0.153
3k	21.8 ± 2.0	4.662	5	0.161
3m	39.8 ± 2.3	4.34	5	0.134
3o	57.4 ± 1.2	4.241	5	0.164
3p	47.9 ± 5.5	4.32	5	0.206
3q	27.5 ± 0.1	4.561	5	0.154
4a	73.6 ± 7.5	4.134	5	0.07
4b	77.4 ± 6.2	4.111	6	0.091
4d	63.8 ± 4.5	4.195	5	0.068
5b	70.5 ± 2.1	4.152	5	0.09
6a	42.0 ± 1.6	4.377	6	0.178
6b	39.3 ± 0.1	4.406	6	0.173
7a	16.4 ± 0.3	4.784	4	0.22
7b	27.2 ± 1.1	4.565	4	0.283
7c	27.1 ± 0.7	4.567	5	0.227
7d	10.2 ± 0.6	4.99	4	0.247
7e	14.8 ± 1.9	4.831	4	0.077

GFA equation:

$$\text{pIC}_{50} = 3.8276 + 0.2744 * \text{Count}\langle\text{EPFP}_6\text{:}-66486510\rangle + 0.52132 * \text{Count}\langle\text{EPFP}_6\text{:}838692040\rangle + 0.3257 * \text{Count}\langle\text{EPFP}_6\text{:}-653303157\rangle - 0.0035719 * \text{Molecular_PolarSurfaceArea} + 0.43089 * \langle 5.2815 - \text{Num_RotatableBonds} \rangle$$

Parameter values generated: n (number of compounds in analysis)=25; $r^2 = 0.9681$; $r^2(\text{adj}) = 0.9535$; $r^2(\text{pred}) = 0.9182$; RMS (root mean square) residual error = 0.0507; Friedman L.O.F (lack of fit) = 0.0199; and q^2 (cross validation correlation coefficient)=0.6110.

The term EPFP_6 is a fingerprint for molecular characterization. The use of this descriptor in model generation allows the identification of the molecular features that favor inhibition and are non-promoting. Num_rotatableBonds is the number of rotatable bonds, and Molecular_FractionalPolarSurfaceArea (MFPSA) is the total surface belonging to polar atoms and is calculated as the ratio of the polar surface area divided by the total surface area. These types of descriptors permit us to predict the transport properties of drugs.

Both the fingerprint EPFP_6, and Num_rotatableBonds show positive effects on the NO-inhibitory potency, whereas molecular_FractionalPolarSurfaceArea has the opposite effect. Based on the GFA equation, 95.35% of the variance (adjusted

coefficient of variation) and the LOO-predicted variance was found to be 61.10%; the lower Friedman L.O.F value of 0.0199 signifies that the GFA model fitted the data well.

According to the GFA equation, three dominant molecular fragments (Fig. 3) were determined by this model. All of the molecular fragments, **A** (EPFP_6: -66486510), **B** (EPFP_6: 838692040) and **C** (EPFP_6: -653303157), have positive regression coefficients, indicating that all three features are important for the inhibition potency. Molecular fragment B, with a hydroxyl group at the *para*-position in ring B, enhances the NO-inhibitory activity more than the fragments A and C. This trend has been substantiated by demethylated compounds **7a**, **7d** and **7e**, which displayed stronger activity than that of their respective methoxy-containing diarylpentadienone (compounds **3b**, **3l** and **3c**).

The number of rotatable bonds is also an important descriptor influencing the activity. GFA analysis suggested that the number of rotatable bond present in the diarylpentadienone system should never be higher than five, above which causes NO inhibition by the molecules.

Additionally, the higher value of MFPSA is undesirable for potency of the compounds. The effect of this factor is demonstrated by comparing the NO inhibitory activities of compounds **1a**, **1j** and **1k**, which clearly indicated that the presence of a heterocyclic ring moiety lowered the activity. However, this MFPSA descriptor only plays a minor role in the activity because of its relatively small coefficient value. In contrast, fragment B of the EPFP fingerprint plays a larger role in enhancing NO inhibition. This trend is displayed by the most potent candidates, compound **7d**.

A randomization test at a 95% confidence level was performed to determine the significance and reliability of the generated GFA data, and the results are shown in Table 3. The resulting random r^2 value of 0.7798 is considerably lower than the non-random r^2 value of 0.9682 from the GFA equation, suggesting that the model generated was significant and was not obtained by chance.

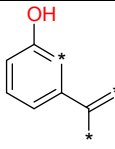
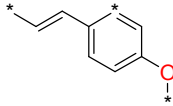
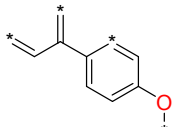
EPFPs code	Fragment fingerprint	Regression coefficient
A EPFP_6: - 66486510		+ 0.2744
B EPFP_6: 838692040		+ 0.52132
C EPP_6: - 653303157		+ 0.3257

Fig. 3 EPFPs equation descriptors

Table 3. Randomization test of GFA equation.

Eq. No.	Model 1
r^2 from non-random model	0.9681
Confidence level	95%
Total trials	49
Non-random $r^2 <$ random r^2	49
Mean value of r^2 form random trials	0.7798
Standard deviation of random trials	± 0.17

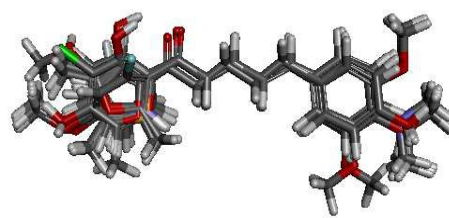
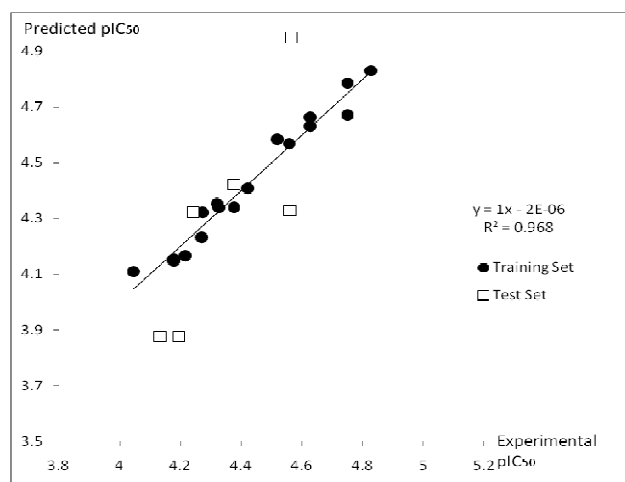
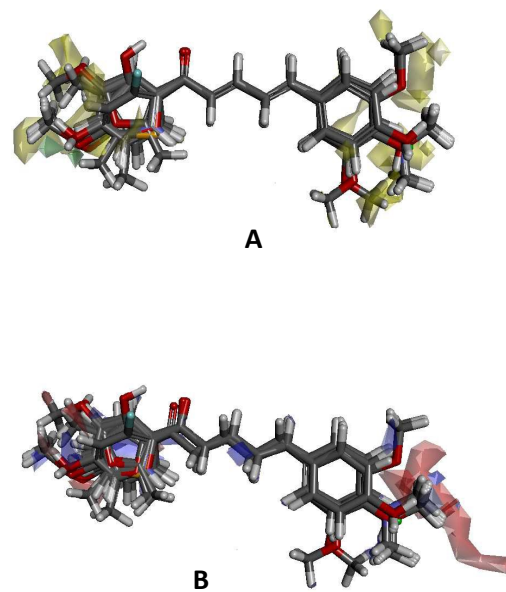
3D QSAR

The use of 3D-QSAR analysis employing the comparative molecular field analysis (CoMFA) method facilitated the correlation of the biological activity with the 3D structures of potential drug molecules as well as the van der Waals potentials and Coulombic terms, which represent the steric and electrostatic potential factors.

Partial least squares (PLS) analysis was used to linearly correlate the CoMFA interaction energies and the inhibitory activity. The IC_{50} values were converted into pIC_{50} ($-\log IC_{50}$) and used as the dependent variables in the 3D QSAR analysis. The steric and electrostatic CoMFA potentials were calculated at each lattice intersection of a regularly spaced grid of 1.0 Å. The most potent compound in the series, compound **7d**, was used as a template, and the rest of the molecules were aligned at the common α,β -unsaturated ketone fragment using a docking method. The final, aligned conformation of all ligands is displayed in Fig. 4.

From the total of 25 compounds involved in this analysis, 17 molecules were incorporated into the training set and eight candidates were in the test set in order to generate the CoMFA model (Table 2). The statistical validity of the model generated was judged by the high values of q^2 (more than 0.5) and r^2 (more than 0.9). The 3D-QSAR model gave a high cross-validated q^2 value of 0.536 and a non-cross-validated correlation coefficient r^2 of 0.988, which signified the correlation. A graph depicting the actual versus predicted activity of the training set and the test set compounds is shown in Fig. 5. The CoMFA contour maps developed were displayed in Fig. 6A and Fig. 6B, denoting the steric and electrostatic potential factors, respectively.

In Fig. 6B, the blue region represents the favorable electrostatic area with positive charge, whereas the red region indicates the favorable electrostatic area with negative charge.²⁵ There is a major red region around C-4' of ring B in the electrostatic map, suggesting that a substituent with a negative charge on the ring system would result in higher potency. The presence of electron-donating groups, such as the 4'-OH moiety in ring B, enhances the anti-inflammatory activity, as demonstrated by compounds **3h**, **7a** and **7d**. In contrast, the analogues containing 4'-Cl, 4'-N(CH₃)₂ and 3',5'-OCH₃,4'-OH in ring B were found to be weak, as shown by compounds in series 4, 5 and 6. This finding is in agreement with the results of 2D QSAR analysis earlier, where compounds possessing molecular fragment **B** showed higher bioactivity. In the steric contour map (Fig. 6A), no green region is observed, indicating that a bulky substituent is not favorable to increase the NO-inhibition activity. Additionally, the heavy yellow shadow on C-2,4 on ring A and C-3',4',5' of ring B implied that a less bulky functional group is preferred to enhance the activity.

**Fig. 4** Structural alignment of compounds using template-based technique based on core of analogue **7d****Fig. 5** The actual versus predicted activity of training and test sets**Fig. 6** (A) Steric contour maps. Green region represent favorable bulky groups region, while yellow maps represent disfavorable bulky group area. (B) Electrostatic potential contour maps. Blue region indicate positive charge electrostatic favorable areas whereas, red contour electronegative groups are favorable in enhancing activity.

ADMET Analysis

ADMET analysis is a computationally designed tool for predicting pharmacokinetic properties, including absorption, distribution, metabolism, excretion and toxicity, for a collection of molecules based on their molecular structure within an organism. This ADMET prediction is crucial in drug discovery and development to improve the efficiency of drug candidates and to reduce the cost and time by optimizing the screening and testing only on the most promising compounds with acceptable properties.

The ADMET analysis of ten selected molecules was performed on six important parameters, including the aqueous solubility (AS), human intestinal absorption (HIA), blood–brain barrier (BBB), cytochrome P450 2D6 (CYP2D6), plasma protein binding (PPB), and hepatotoxicity (HT), via Discovery Studio 3.1. The ADMET prediction results were compiled in Table 4.

According to Lipinski,²⁶ solubility is still the most important issue in drug discovery because many negative impacts can be intensified by lower-solubility drug-like molecules, including relatively poor absorption and bioavailability after oral dosing. Thus, improved absorption and solubility are necessary to enhance the pharmacokinetic properties in the human body.

Based on the ADMET findings, compounds **1c**, **7a**, **7b**, and **7c** displayed sufficient aqueous solubility and intestinal absorption, indicating that they can serve as good oral drugs, in comparison to **3h-k**, **7d**, and **7e** that had poor aqueous solubility.

The blood–brain barrier (BBB) is normally associated with the delivery process involved in central nervous system (CNS). The BBB penetration implies the ability of drug-like molecules to pass through the blood–brain barrier to reach their therapeutic target in the brain. High BBB permeation is crucial for CNS-active compounds but is undesirable for CNS-inactive compounds in order to avoid CNS side effects.²⁷ As shown in Table 4, all the ten compounds possessed medium to very high BBB penetration, signifying that they are effective candidates for treating CNS related disorders.

Cytochrome P450 2D6 (CYP2D6) is an enzyme involved in the metabolism of drugs in the liver, and its inhibition is usually caused by the drug–drug interactions. These drug–drug interactions normally occur when two drugs are orally co-administered and compete for the same metabolizing enzyme (involved in ADME), causing one drug to be bound by isozyme, while the other drug is excluded from metabolism.²⁸ Notably, whenever the drug is metabolized too quickly, the drug potency will decrease, but when the drug is metabolized too slowly, the concentration may increase to a toxic level. As presented, all compounds show negative results for CYP2D6 inhibition, indicating their tolerance towards CYP2D6.

Plasma proteins may adsorb a significant amount of drug molecules once they have entered the bloodstream and to be distributed to their specific therapeutic targets. Protein plasma binding (PPB) can affect the pharmacokinetics of drug substances because the bound molecules are temporarily shielded from metabolism. Hence, only the unbound drugs exhibit noteworthy pharmacological effects. In this experiment, all compounds displayed strong binding interactions between the drug molecules and plasma protein, which suggested that dosing issues must be addressed to achieve the desirable therapeutic concentration for treatment. The last descriptor to be considered is hepatotoxicity, which predicts the potential organ

toxicity caused by the drug-like molecules (e.g., liver injury). All compounds except **1c** and **3h** are hepatotoxins based on the calculated results.

TOPKAT Analysis

Safe drugs with minimal deleterious side effects still remain the major goal of medicinal chemistry. Additional toxicology studies must be run to assess the potential toxicities caused by drugs, as they may lead to drug-candidate attrition during preclinical and clinical development.²⁹ To improve the efficiency of drug discovery, analysis is conducted using Toxicity Prediction by Komputer Assisted Technology (TOPKAT). The main goal of this analysis is to determine the potential ecotoxicity, toxicity, mutagenicity, and reproductive or developmental toxicity of the selected compounds.

Table 4. Result of ADMET predictions on selected parameters of selected compounds.

	AS	HIA	BBB	CYP2D6	HT	PPB
3	Good	Good	High	Non-inhibit	Non-hepatotoxin	Bound
20	Low	Good	High	Non-inhibit	Non-hepatotoxin	Bound
21	Low	Good	High	Non-inhibit	Hepatotoxin	Bound
22	Low	Good	High	Non-inhibit	Hepatotoxin	Bound
23	Low	Good	High	Non-inhibit	Hepatotoxin	Bound
41	Good	Good	High	Non-inhibit	Hepatotoxin	Bound
42	Good	Good	Medium	Non-inhibit	Hepatotoxin	Bound
43	Good	Good	Medium	Non-inhibit	Hepatotoxin	Bound
45	Low	Good	High	Non-inhibit	Hepatotoxin	Bound
46	Low	Good	Very high	Non-inhibit	Hepatotoxin	Bound

AS = aqueous solubility; HIA = human intestinal absorption; BBB = blood brain barrier; CYP2D6 = cytochrome P450 2D6; PPB = protein plasma binding; HT = hepatotoxicity

Toxicity studies (TOPKAT) follow the same procedure as used in calculating the ADMET properties. In this study, the same ten selected molecules were analyzed using toxicity predictors, including the aerobic biodegradability, mutagenicity, rodent carcinogenicity, ocular irritancy, skin irritancy and skin sensitization. The results of TOPKAT are presented in Table 5.

Based on the toxicity-prediction findings, all of the selected compounds are nonmutagenic, and nonbiodegradable, except for compound **3h**. Unfortunately, compounds **7a** and **7d** are predicted to be carcinogenic. In addition, all candidates are skin sensitizers, and compounds **3h-k**, **7d**, and **7e** are ocular irritants. Compounds **7d** and **7e** are expected to exhibit skin irritancy.

In an attempt to develop new NO inhibitors as potent anti-inflammatory agents, a series of 1,5-diphenylpenta-2,4-dien-1-one analogues were synthesized and evaluated for their biological activities. Compound **7d** is the most promising NO inhibitor from the entire series. The combination of two computational techniques, the 2D and 3D QSAR has helped provide the most significant correlation of structural descriptors and steric and electrostatic

factors with the biological reactivity. In addition, ADMET and TOPKAT analyses facilitated the understanding of the drug efficiency and possible toxicity of each compounds. The information obtained in this study suggested that the *para*-hydroxyl group on ring B and an α,β -unsaturated ketone moieties are important for the NO-inhibition activity.

Table 5. Result of TOPKAT analysis of selected compounds.

	AB	AM	RC	OI	SI	SS
3	Non-Degradable	Non-Mutagen	Non-Carcinogen	Non-Irritant	Non-Irritant	Non-Sensitizer
20	Degradable	Mutagen	Carcinogen	Irritant	Irritant	Sensitizer
21	Non-Degradable	Non-Mutagen	Non-Carcinogen	Non-Irritant	Non-Irritant	Non-Sensitizer
22	Degradable	Mutagen	Carcinogen	Irritant	Irritant	Sensitizer
23	Non-Degradable	Non-Mutagen	Non-Carcinogen	Non-Irritant	Non-Irritant	Non-Sensitizer
41	Degradable	Mutagen	Carcinogen	Irritant	Irritant	Sensitizer
42	Non-Degradable	Non-Mutagen	Non-Carcinogen	Non-Irritant	Non-Irritant	Non-Sensitizer
43	Degradable	Mutagen	Carcinogen	Irritant	Irritant	Sensitizer
45	Non-Degradable	Non-Mutagen	Non-Carcinogen	Non-Irritant	Non-Irritant	Non-Sensitizer
46	Degradable	Mutagen	Carcinogen	Irritant	Irritant	Sensitizer

AB = aerobic biodegradability; AM = Ames mutagenicity; RC = rodent carcinogenicity; OI = ocular irritancy; SI = skin irritancy; SS = skin sensitization

Chemical stability test

There are several drawbacks that limit the potential development of curcumin as a therapeutic agent. Various clinical studies strongly indicate that one such drawback is its low stability. Stability of a compound in solution is necessary for in vivo oral dosing, particularly in acidic, basic and physiological conditions of the gastrointestinal (GI) tract in order to improve compounds pharmacokinetic (PK) performance and the in vivo pharmacological activity. Therefore, we tested the chemical stability of the most active compound, **7d** and curcumin in phosphate buffer containing 1% DMSO in different pH's including the acidic (pH 2.4), physiological (pH 7.0) and basic (pH 12.7) conditions, using an absorption spectrum assay. Fig. 7 illustrates the changes in ultraviolet absorptions of curcumin and compound **7d**, respectively. Curcumin is very stable in acidic environment, but the poor chemical stability of curcumin could be observed from its maximal absorption peaks gradually decreased over time at pH 7. However, the stability of curcumin is increases at higher pH (>11.7). Conversely, the absorption peak of the compound **7d** showed no significant changes in all different pH conditions, which indicated that our most active compound was chemically more stable in vitro, in comparison to curcumin.

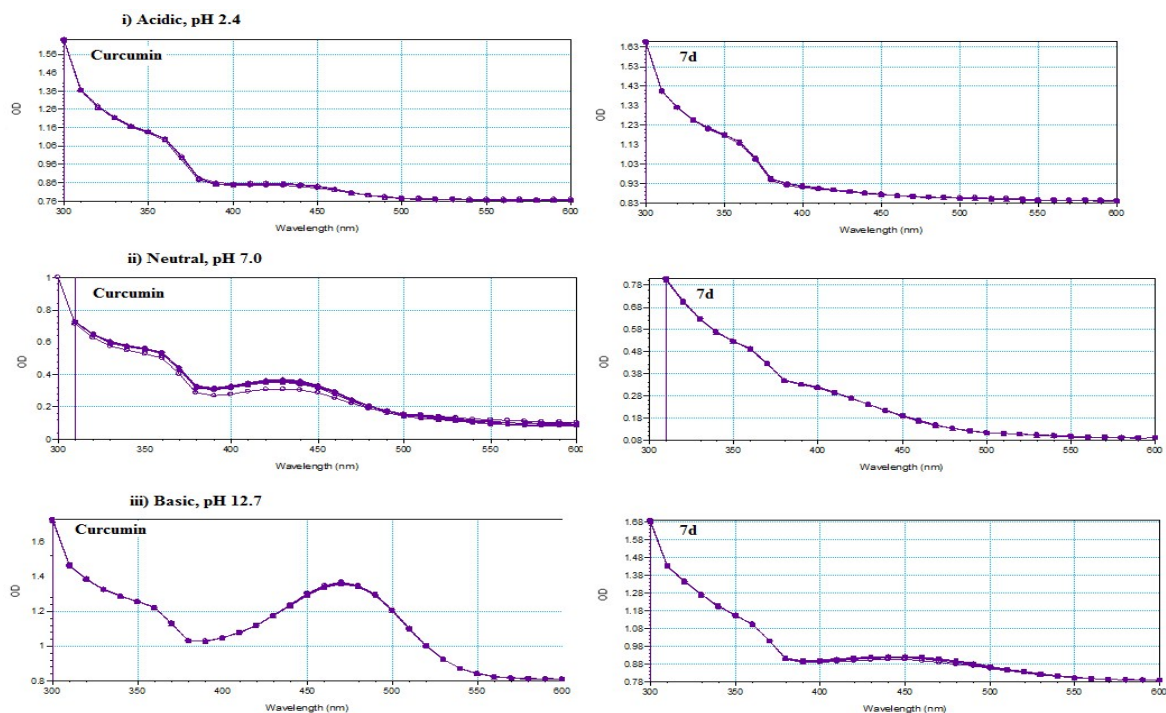


Fig. 7 Ultraviolet-visible absorption spectra of curcumin and **7d** at different pH

Conclusions

In an attempt to develop new NO inhibitors as potent anti-inflammatory agents, a series of 1,5-diphenylpenta-2,4-dien-1-one analogues were synthesized and evaluated for their biological activities. Compound 7d is the most promising NO inhibitor from the entire series. The combination of two computational techniques, the 2D and 3D QSAR has helped provide the most significant correlation of structural descriptors and steric and electrostatic factors with the biological reactivity. In addition, ADMET and TOPKAT analyses facilitated the understanding of the drug efficiency and possible toxicity of each compounds. The information obtained in this study suggested that the *para*-hydroxyl group on ring B and an α,β -unsaturated ketone moieties are important for the NO-inhibition activity.

Experimental

Materials and instrumentations

All chemicals and reagents were purchased from Merck, Sigma-Aldrich and Thermo Fischer Scientific. All solvents were dried and distilled prior to use. The solvents used in the spectroscopic measurements were of spectroscopic grade. The reaction mixtures were extracted with organic solvents, dried over anhydrous magnesium sulfate and then concentrated in vacuo. To monitor the progress of a reaction, thin-layer chromatography was performed on aluminum TLC sheets of silica gel 60 F254 (layer thickness 0.2 mm) from Merck. Column chromatography purification was performed on silica gel 60 (70-230 mesh ASTM, Merck). Mass spectra were measured on a GCMS-QP5050A (Shimadzu, Kyoto, Japan) Mass Spectrometer. High-resolution MS (HRMS) was determined using Acquity Ultra-performance Liquid Chromatography (UPLC)-PDA system coupled to Synapt High-Definition Mass Spectrometry (HDMS) quadrupole-orthogonal acceleration time-of-flight (oaTOF) detector (Waters Corporation, USA) and equipped with an ESI source. Nuclear magnetic resonance spectra were recorded using a Varian 500 MHz NMR Spectrometer (Varian Inc., Palo Alto, CA), and the melting points were determined using a Fisher-Johns melting point apparatus.

Chemistry

General procedure for the synthesis of I (Series 1-6). Equimolar quantities of the appropriate cinnamaldehyde (2 mmol) and substituted acetophenone (2 mmol) were dissolved in 5 ml ethanol. The resulting mixture was stirred for 5 min, and then 1 ml of 6M NaOH was added dropwise over three minutes. After the addition was completed, the reaction mixture was stirred overnight at room temperature. The adduct solution was poured into crushed ice and neutralized with diluted HCl. The solution was extracted by ethyl acetate (3 x 10 ml). The organic layer was dried over anhydrous MgSO₄ and evaporated under reduced pressure. Finally, the crude products were purified by column chromatography.³⁰ The purity of all compounds were >95% based on HPLC analysis.

1,5-Diphenylpenta-2,4-dien-1-one (1a)

Yellow solid (47.8%), m.p. 102-103 °C (lit.³¹ 102-103 °C). ¹H NMR (500 MHz, CDCl₃, δ ppm): 7.02 - 7.07 (*m*, 2H, 3-H, 4-H), 7.10 - 7.13 (*d*, 1H, 1-H), 7.32 - 7.43 (*m*, 3H, 3''-H, 4''-H, 5''-H), 7.48 - 7.55 (*m*, 4H, 3'-H, 5'-H, 2''-H, 6''-H), 7.58 (*d*, *J* = 7.3 Hz, 1H, 4'-H), 7.59 - 7.65 (*m*, 1H, 2-H), 7.99 (*d*, *J* = 7.02 Hz, 2H, 2'-H, 6'-H). ¹³C NMR (126 MHz, CDCl₃, δ ppm): 190.5 (C=O), 144.9 (C-2), 141.9 (C-4), 138.2 (C-1'), 136.1 (C-1''), 133.1 (C-4'), 128.9 (C-4''), 128.5 (C-3''),

C-5''), 128.4 (C-3', C-5'), 128.2 (C-2', C-6'), 127.3 (C-2'', C-6''), 126.9 (C-3), 125.4 (C-1). EIMS, *m/z*: 234 (M⁺).

(3-Hydroxyphenyl)-5-phenylpenta-2,4-dien-1-one (1c)

Yellow solid (21.2%), m.p. 115-116 °C. ¹H NMR (500 MHz, CDCl₃, δ ppm): 6.36 (*br. s*, 1H, 5'-OH), 7.03 - 7.06 (*m*, 2H, 3-H, 4-H), 7.09 (*d*, 1H, 1-H), 7.34 - 7.39 (*m*, 5H, 2''-H, 3''-H, 4''-H, 5''-H, 6''-H), 7.50 - 7.54 (*m*, 3H, 2'-H, 3'-H, 4'-H), 7.59 (*s*, 1H, 6'-H), 7.60 - 7.65 (*m*, 1H, 2-H). ¹³C NMR (126 MHz, CDCl₃, δ ppm): 190.7 (C=O), 156.4 (C-5'), 145.5 (C-2), 142.5 (C-4), 139.5 (C-1'), 136.0 (C-1''), 129.9 (C-3'), 129.3 (C-4''), 128.9 (C-3'', C-5''), 127.4 (C-2'', C-6''), 126.8 (C-3), 125.2 (C-1), 120.9 (C-2'), 120.3 (C-4'), 115.0 (C-6'). EIMS, *m/z*: 250 (M⁺), HRESIMS *m/z* 249.0997 [M-H]⁻ (calculated for C₁₇H₁₄O₂, 249.0994).

(3-Hydroxy-4-methoxyphenyl)-5-(4-methoxyphenyl)penta-2,4-dien-1-one (3h)

Yellow solid (54.9%), m.p. 72-73 °C. ¹H NMR (500 MHz, acetone-d₆, δ ppm): 3.83 (*s*, 3H, 4''-OCH₃), 3.93 (*s*, 3H, 4'-OCH₃), 6.91 - 7.01 (*m*, 3H, 3'-H, 3-H, 4-H), 7.08 (*d*, *J* = 4.4 Hz, 2H, 3''-H, 5''-H), 7.31 (*d*, *J* = 14.7 Hz, 1H, 1-H), 7.55 (*d*, *J* = 7.8 Hz, 3H, 6'-H, 2''-H, 6''-H), 7.61 - 7.69 (*m*, 2H, 2-H, 2'-H), 8.73 (*br. s*, 1H, 5'-OH). ¹³C NMR (126 MHz, acetone-d₆, δ ppm): 187.1 (C=O), 160.5 (C-4''), 151.3 (C-4'), 147.6 (C-5'), 143.5 (C-2), 140.6 (C-4), 130.6 (C-1'), 129.1 (C-3), 128.6 (C-2'', C-6''), 125.1 (C-1), 124.1 (C-1''), 123.0 (C-2'), 114.5 (C-6'), 114.2 (C-3'', C-5''), 111.0 (C-3'), 55.3 (4''-OCH₃), 54.7 (4'-OCH₃). EIMS, *m/z*: 310 (M⁺), HRESIMS *m/z* 309.1209 [M-H]⁻ (calculated for C₁₉H₁₈O₄, 309.1205).

(4-Hydroxy-3,5-dimethoxyphenyl)-5-(4-methoxyphenyl)penta-2,4-dien-1-one (3i)

Yellowish orange solid (15.4%), m.p. 90-91 °C. ¹H NMR (500 MHz, acetone-d₆, δ ppm): 3.97 (*s*, 3H, 4''-OCH₃), 4.05 (*s*, 6H, 3'-, 5'-OCH₃), 7.10 (*d*, *J* = 8.6 Hz, 2H, 3''-H, 5''-H), 7.18 - 7.23 (*m*, 2H, 1-H, 4-H), 7.42 - 7.50 (*m*, 1H, 3-H), 7.53 (*s*, 2H, 2'-H, 6'-H), 7.63 - 7.71 (*m*, 3H, 2-H, 2''-H, 6''-H), 8.25 (*br. s*, 1H, 4'-OH). ¹³C NMR (126 MHz, acetone-d₆, δ ppm): 187.2 (C=O), 160.6 (C-4''), 147.7 (C-3', C-5'), 143.7 (C-2), 141.0 (C-4), 140.7 (C-4'), 129.2 (C-2'', C-6''), 129.1 (C-1'), 128.7 (C-1''), 125.1 (C-1), 124.2 (C-3), 114.3 (C-3'', C-5''), 106.2 (C-2', C-6'), 55.8 (3', 5'-OCH₃), 54.8 (4''-OCH₃). EIMS, *m/z*: 340 (M⁺), HRESIMS *m/z* 339.1314 [M-H]⁻ (calculated for C₂₀H₂₀O₅, 339.1311).

(3-Chloro-4-hydroxyphenyl)-5-(4-methoxyphenyl)penta-2,4-dien-1-one (3j)

Yellow solid (34.7%), m.p. 143-144 °C. ¹H NMR (500 MHz, CDCl₃, δ ppm): 3.85 (*s*, 3H, 4''-OCH₃), 6.11 (*br. s*, 1H, 4'-OH), 6.90 - 6.93 (*m*, 3H, 4-H, 3''-H, 5''-H), 6.98 - 7.02 (*m*, 2H, 1-H, 3-H), 7.11 (*d*, *J* = 8.6 Hz, 1H, 3'-H), 7.45 (*d*, *J* = 8.3 Hz, 2H, 2''-H, 6''-H), 7.59 - 7.64 (*m*, 1H, 2-H), 7.86 (*d*, *J* = 8.6 Hz, 1H, 2'-H), 8.04 (*s*, 1H, 6'-H). ¹³C NMR (126 MHz, CDCl₃, δ ppm): 183.1 (C=O), 159.1 (C-4'), 156.4 (C-4''), 139.7 (C-2), 136.7 (C-4), 129.2 (C-2'', C-6''), 127.0 (C-1', C-1''), 126.1 (C-3), 124.9 (C-6'), 124.5 (C-1), 120.9 (C-5'), 119.9 (C-3'), 111.9 (C-2'), 110.0 (C-3'', C-5''), 50.8 (4''-OCH₃). EIMS, *m/z*: 314.5 (M⁺), HRESIMS *m/z* 313.0712 [M-H]⁻ (calculated for C₁₈H₁₅ClO₃, 313.0710).

(2-Fluoro-4-hydroxyphenyl)-5-(4-methoxyphenyl)penta-2,4-dien-1-one (3k)

Orange solid (51.1%), m.p. 150-151 °C. ¹H NMR (500 MHz, acetone-d₆, δ ppm): 3.84 (*s*, 3H, 4''-OCH₃), 6.68 (*dd*, *J* = 13.0, 2.0 Hz, 1H, 5'-H), 6.80 (*dd*, *J* = 8.6, 2.0 Hz, 1H, 3'-H), 6.97 (*d*, *J* = 8.6 Hz, 3H, 3''-H, 5''-H), 7.00 (*d*, *J* = 2.7 Hz, 1H, 1-H), 7.05 - 7.14 (*m*, 2H, 3-H, 4-H), 7.38 (*br. s*, 1H, 4'-OH), 7.51 (*dd*, *J* = 14.8, 8.2 Hz, 1H, 2-H), 7.57 (*d*, *J* = 8.6 Hz, 2H, 2''-H, 6''-H), 7.72 - 7.80 (*t*, 1H, 2'-H). ¹³C NMR (126 MHz, acetone-d₆, δ ppm): 185.8 (C=O), 162.8 (C-4'), 161.6 (C-6'), 160.5 (C-4''), 143.8 (C-2), 141.1 (C-4), 128.9 (C-2'), 128.6 (C-2'', C-6''), 127.6 (C-1''), 127.6 (C-3), 124.7 (C-1), 118.4 (C-1'), 114.0 (C-3'', C-5''), 111.9 (C-3'), 102.8 (C-5'), 54.6

(4''-OCH₃). EIMS, m/z: 298 (M⁺), HRESIMS m/z 297.1007 [M-H]⁻ (calculated for C₁₈H₁₅FO₃, 297.1005).

General procedure for the synthesis of II (Series 7). The methoxylated diarylpentanoids (I, 0.5 mmole), was dissolved in 10 ml of dichloromethane. To it 1.5 ml of boron tribromide was added slowly and stirred for 1h and continued for overnight at room temperature. The reaction solution was then poured into crushed ice, extracted with ethyl acetate and dried over anhydrous MgSO₄. The organic layer was concentrated under vacuum and the resulting products were purified using column chromatography under appropriate solvent system.³²

1,5-Bis(4-hydroxyphenyl)penta-2,4-dien-1-one. (7a)

Yellow solid (30.7%), m.p. 173-174°C. ¹H NMR (500 MHz, acetone-d₆, δ ppm): 6.88 (*d*, *J* = 8.3 Hz, 2H, 3''-H, 5''-H), 6.96 (*d*, *J* = 8.6 Hz, 2H, 3'-H, 5'-H), 7.02 - 7.08 (*m*, 2H, 3-H, 4-H), 7.26 (*d*, *J* = 15.0 Hz, 1H, 1-H), 7.48 (*d*, *J* = 8.6 Hz, 2H, 2''-H, 6''-H), 7.50 - 7.58 (*m*, 1H, 2-H), 7.98 (*d*, *J* = 8.6 Hz, 2H, 2'-H, 6'-H), 8.87 (*br. s.*, 1H, 4''-OH), 9.32 (*br. s.*, 1H, 4'-OH). ¹³C NMR (126 MHz, acetone-d₆, δ ppm): 187.2 (C=O), 161.7 (C-4'), 158.7 (C-4''), 143.9 (C-2), 141.2 (C-4), 130.6 (C-2', C-6'), 130.4 (C-1'), 128.9 (C-2'', C-6''), 128.2 (C-1''), 124.5 (C-3), 123.8 (C-1), 115.8 (C-3', C-5'), 115.3 (C-3'', C-5''). EIMS, m/z: 266 (M⁺), HRESIMS m/z 265.0947 [M-H]⁻ (calculated for C₁₇H₁₄O₃, 265.0943).

(2,4-Dihydroxyphenyl)-5-(4-hydroxyphenyl)penta-2,4-dien-1-one (7b)

Orange solid (22.0%), m.p. 134-135°C. ¹H NMR (500 MHz, acetone-d₆, δ ppm): 6.37 (*s*, 1H, 5'-H), 6.48 (*d*, *J* = 8.8 Hz, 1H, 3'-H), 6.90 (*d*, *J* = 6.8 Hz, 2H, 3''-H, 5''-H), 7.04 - 7.20 (*m*, 2H, 1-H, 3-H), 7.36 (*d*, *J* = 14.7 Hz, 1H, 4-H), 7.51 (*d*, *J* = 6.8 Hz, 2H, 2''-H, 6''-H), 7.61 - 7.73 (*m*, 1H, 2-H), 7.95 (*d*, *J* = 8.3 Hz, 1H, 2'-H), 8.95 (*br. s.*, 1H, 4''-OH), 9.66 (*br. s.*, 1H, 4'-OH), 13.63 (*br. s.*, 1H, 6'-OH). ¹³C NMR (126 MHz, acetone-d₆, δ ppm): 187.1 (C=O), 161.6 (C-4', C-6'), 158.5 (C-4''), 143.7 (C-2), 141.0 (C-4), 130.4 (C-2'), 130.1 (C-2'', C-6''), 128.7 (C-1''), 127.9 (C-3), 124.2 (C-3'', C-5''), 123.6 (C-1), 115.6 (C-1'), 115.0 (C-3', C-5'). EIMS, m/z: 282 (M⁺), HRESIMS m/z 281.0895 [M-H]⁻ (calculated for C₁₇H₁₄O₄, 281.0892).

(2-Hydroxy-4-methoxyphenyl)-5-(4-hydroxyphenyl)penta-2,4-dien-1-one (7c)

Brown solid (67.7%), m.p. 192-193°C. ¹H NMR (500 MHz, acetone-d₆, δ ppm): 3.90 (*s*, 3H, 4'-OCH₃), 6.48 (*s*, 1H, 5'-H), 6.54 (*d*, *J* = 8.8 Hz, 1H, 3'-H), 6.91 (*d*, *J* = 8.3 Hz, 2H, 3''-H, 5''-H), 7.06 - 7.21 (*m*, 2H, 1-H, 3-H), 7.38 (*d*, *J* = 14.7 Hz, 1H, 4-H), 7.52 (*d*, *J* = 8.3 Hz, 2H, 2''-H, 6''-H), 7.65 - 7.74 (*m*, 1H, 2-H), 8.00 (*d*, *J* = 8.8 Hz, 1H, 2'-H), 8.91 (*br. s.*, 1H, 4''-OH), 13.69 (*br. s.*, 1H, 6'-OH). ¹³C NMR (126 MHz, acetone-d₆, δ ppm): 187.1 (C=O), 166.5 (C-4', C-6'), 164.7 (C-4''), 144.9 (C-2), 142.2 (C-4), 131.8 (C-2'), 129.0 (C-2'', C-6''), 127.8 (C-1''), 124.0 (C-3), 122.2 (C-1), 115.7 (C-3'', C-5''), 115.4 (C-1'), 107.8 (C-3'), 102.7 (C-5'), 55.3 (4'-OCH₃). EIMS, m/z: 296 (M⁺), HRESIMS m/z 295.1053 [M-H]⁻ (calculated for C₁₈H₁₆O₄, 295.1049).

5-(4-Hydroxyphenyl)-1-(5-methylthiophen-2-yl)penta-2,4-dien-1-one (7d)

Dark green solid (52.9%), m.p. 135-137°C. ¹H NMR (500 MHz, acetone-d₆, δ ppm): 2.88 (*s*, 3 H, 4'-CH₃), 6.89 (*d*, *J* = 8.3 Hz, 2H, 3''-H, 5''-H), 6.94 (*d*, *J* = 3.2 Hz, 1H, 3'-H), 6.98 - 7.05 (*m*, 1H, 1-H), 7.06 - 7.15 (*m*, 2H, 3-H, 4-H), 7.44 - 7.51 (*m*, 2H, 2''-H, 6''-H), 7.51-7.56 (*m*, 1H, 2-H), 7.77 (*d*, *J* = 3.7 Hz, 1H, 2'-H), 8.78 (*br. s.*, 1H, 4''-OH). ¹³C NMR (126 MHz, acetone-d₆, δ ppm): 181.2 (C=O), 160.5 (C-4''), 149.6 (C-1'), 144.0 (C-2), 143.7 (C-4), 141.6 (C-4'), 132.0 (C-2'), 129.0 (C-1''), 128.8 (C-2'', C-6''), 126.9 (C-3), 124.7 (C-3'), 123.8 (C-1), 114.3 (C-3'', C-5''), 16.1 (4'-CH₃). EIMS, m/z:

270 (M⁺), HRESIMS m/z 269.0717 [M-H]⁻ (calculated for C₁₆H₁₄O₂S, 269.0715).

(4-Fluorophenyl)-5-(4-hydroxyphenyl)penta-2,4-dien-1-one (7e)

Yellow solid (21.9%), m.p. 155-156°C. ¹H NMR (500 MHz, acetone d₆, δ ppm): 6.89 (*d*, *J* = 8.6 Hz, 2H, 3''-H, 5''-H), 7.03 - 7.14 (*m*, 2H, 1-H, 3-H), 7.22 - 7.36 (*m*, 3H, 4-H, 3'-H, 5'-H), 7.49 (*d*, *J* = 8.3 Hz, 2H, 2''-H, 6''-H), 7.54 - 7.66 (*m*, 1H, 2-H), 8.13 (*dd*, *J* = 17.6, 8.4 Hz, 2H, 2'-H, 6'-H), 8.82 (*br. s.*, 1H, 4''-OH). ¹³C NMR (126 MHz, acetone-d₆, δ ppm): 189.0 (C=O), 166.6 (C-4'), 160.9 (C-4''), 145.8 (C-2), 142.3 (C-4), 131.1 (C-1'), 131.0 (C-1''), 129.1 (C-2', C-6'), 128.7 (C-2'', C-6''), 124.9 (C-3), 123.9 (C-1), 115.7 (C-3', C-5'), 114.6 (C-3'', C-5''). EIMS, m/z: 268 (M⁺), HRESIMS m/z 267.0902 [M-H]⁻ (calculated for C₁₇H₁₃FO₂, 267.0900).

Biology

Cell culture. The RAW 264.7 murine macrophages cells obtained from American Type Culture Collection (ATCC, Rockville, MD) were grown in Dulbecco's Modified Eagle's Medium (DMEM) containing 10% FBS and 1% penicillin/streptomycin in a 95% air and 5% CO₂ atmosphere at 37 °C.¹³

Nitrite determination (Griess Assay). The RAW 264.7 cells at 90-95% confluency were detached and seeded (50000 cells/well) into a 96-well culture plate with 50 μL of DMEM and incubated for 24 h. The cells were then stimulated in 5 mg/mL of LPS (*Escherichia coli*, serotype 0111:B4) and 1 ng/ml of interferon-gamma (IFN-γ) in the presence or absence of test compounds for 17 hours. The nitrite production was then determined by a Griess assay. Briefly, 50 μL of Griess Reagent (1% sulfanilamide and 0.1% *N*-(1-naphthyl)ethylenediamine dihydrochloride in 2.5% phosphoric acid) was added to 50 μL of cell culture supernatant. The optical density was measured at 550 nm with a microplate reader after 5 min of incubation at room temperature.¹³

Cell cytotoxicity determination (MTT assay). To determine that the observed nitric oxide inhibition was not falsely positive due to cytotoxic effects, cytotoxicity assay was also performed following the culture. After removal of the supernatant, 100 μL DMEM and 20 μL of 3-(4,5-dimethylthiazol-2-yl)-2,5-diphenyltetrazolium bromide (MTT, 5 mg/ml) were added to all of the wells. The plate was then incubated in 5 % CO₂ at 37°C for 4 h. The supernatants in all wells were discarded, and the formazan crystals formed were dissolved in dimethyl sulfoxide (DMSO) and further incubated for 15 min at room temperature. The absorbance was measured at 570 nm using a microplate reader.¹³

Computational analysis

2D-QSAR. The QSAR model generated by the genetic function approximation (GFA) technique is used to establish the important features that contribute to the biological activity of a molecule, based on the experimental pIC₅₀ (-log IC₅₀). The descriptors used include the fingerprint EFPF_6, molecular polar surface area and number of rotatable bonds.

3D-QSAR. Partial least squares (PLS) analysis was used to linearly correlate the CoMFA interaction energies and the inhibitory activity. The IC₅₀ values were converted into pIC₅₀ (-log IC₅₀) and used as dependent variables in this 3D QSAR analysis. The steric and electrostatic CoMFA potentials were calculated at each lattice intersection of a regularly spaced grid of 1.0 Å. The most potent compound in the series, compound 7d, was used as a template, and the rest of the molecules were aligned using a docking method.

Then, the training set (17 compounds) and test set (8 compounds) were generated after the minimization of ligands through a CHARMM force field.

ADMET and TOPKAT analysis. The ten-most active compounds were selected to undergo the ADMET analysis using the aqueous solubility (AS), human intestinal absorption (HIA), blood–brain barrier (BBB), cytochrome P450 2D6 (CYP2D6), plasma protein binding (PPB), and hepatotoxicity (HT) descriptors, and a toxicity (TOPKAT) analysis was run based on the aerobic biodegradability, mutagenicity, rodent carcinogenicity, ocular irritancy, skin irritancy and descriptors, and skin sensitization descriptors.

Chemical stability test. Absorbance readings were taken from 300–600 nm using a SpectraMax Plus 384 (Molecular Devices LLC, Sunnyvale, CA, USA). A stock solution of 50 mM of curcumin and compound **7d** were prepared and diluted by phosphate buffer (pH of 2.4, 7.0, and 12.7), containing 1% dimethyl sulfoxide (DMSO), to a final concentration of 20 μM. The ultraviolet absorption spectra were collected for over 30 min at 5-min intervals at 25 °C. All spectral measurements were carried out in a 1 cm path-length quartz cuvette.

Acknowledgements

This study was financially supported by Universiti Putra Malaysia under Research University Grant Scheme (RUGS) (9301700). The first author also gratefully acknowledges support by the Ministry of Education Malaysia for funding her study under SLAB scheme.

Notes and references

^aLaboratory of Natural Products, Institute of Bioscience, Universiti Putra Malaysia, 43400, Serdang, Selangor, Malaysia.

^bDepartment of Chemistry, Faculty of Science, Universiti Putra Malaysia, 43400, Serdang, Selangor, Malaysia.

^cDepartment of Food Science, Faculty of Food Science and Technology, Universiti Putra Malaysia, 43400, Serdang, Selangor, Malaysia.

^dDrug and Herbal Research Centre Faculty of Pharmacy, Universiti Kebangsaan Malaysia, Jalan Raja Muda Abd. Aziz, 50300, Kuala Lumpur, Selangor, Malaysia.

^eDepartment of Biochemistry, Faculty of Biotechnology and Biomolecular Sciences, Universiti Putra Malaysia, 43400, Serdang, Selangor, Malaysia.

^fDepartment of Biomedical Science, Faculty of Medicine and Health Sciences, Universiti Putra Malaysia, 43400, Serdang, Selangor, Malaysia.

† Electronic Supplementary Information (ESI) available: [details of any supplementary information available should be included here]. See DOI: 10.1039/b000000x/

- Y. Yamamoto, and R. B. Gaynor, *J. Clin. Invest.*, 2001, **107**, 135-142.
- H. Y. Chung, H. J. Kim, J. W. Kim, and B. P. Yu, *Ann. N. Y. Acad. Sci.*, 2001, **928**, 327-335.
- H. S. Ban, K. Suzuki, S. S. Lim, S. H. Jung, S. Lee, J. Ji, H. S. Lee, Y. S. Lee, K. H. Shin, and K. Ohuchi, *Biochem. Pharmacol.*, 2004, **67**, 1549-1557.
- P. Ben, J. Liu, C. Lu, Y. Xu, Y. Xin, J. Fu, H. Huang, Z. Zhang, Y. Gao, L. Luo, and Z. Yin, *Int. Immunopharmacol.*, 2011, **11**, 179-186.
- J. Rojas, M. Paya, J. N. Dominguez, and M. Luisa Ferrandiz, *Bioorg. Med. Chem. Lett.*, 2002, **12**, 1951-1954.
- M. V. B. Reddy, T. L. Hwang, Y. L. Leu, W. F. Chiou, and T. S. Wu, *Bioorg. Med. Chem.*, 2011, **19**, 2751-2756.
- B. Orlikova, D. Tasdemir, F. Golais, M. Dicato, and M. Diederich, *Biochem. Pharmacol.*, 2011, **82**, 620-631.
- H. W. D. Matthes, B. Luu, and G. Ourisson, *Phytochem.*, 1980, **19**, 2643-2650.
- H. Mohamad, F. Abas, D. Permana, N. H. Lajis, A. M. Ali, M. A. Sukari, T. Y. Hin, H. Kikuzaki, and N. Nakatani, *Z. Naturforsch. C.*, 2004, **59**, 811-815.
- Y. J. Surh, *Food Chem. Toxicol.*, 2002, **40**, 1091-1097.
- G. Shoba, D. Joy, T. Joseph, M. Majeed, R. Rajendran, and P. S. Srinivas, *Planta Med.*, 1998, **64**, 353-356.
- R. K. Maheshwari, A. K. Singh, J. Gaddipati, and R. C. Simal, *Life Sci.*, 2006, **78**, 2081-2087.
- K. H. Lee, F. H. Ab Aziz, A. Syahida, F. Abas, K. Shaari, D. A. Israf, and N. H. Lajis, *Eur. J. Med. Chem.*, 2009, **44**, 3195-3200.
- S. S. Sardjiman, M. S. Reksohadiprodo, L. Hakim, H. van der Goot, and H. Timmerman, *Eur. J. Med. Chem.*, 1997, **32**, 625-630.
- G. Liang, L. Shao, Y. Wang, C. Zhao, Y. Chu, J. Xiao, Y. Zhao, X. Li, and S. Yang, *Bioorg. Med. Chem.*, 2009, **17**, 2623-2631.
- G. Liang, S. Yang, L. Jiang, Y. Zhao, L. Shao, J. Xiao, F. Ye, Y. Li, and X. Li, *Chem. Pharm. Bull. (Tokyo)*, 2008, **56**, 162-167.
- P. Kulkarni, P. Wagh, and P. Zubaidha, *Chem. J.*, 2012, **2**, 106-110.
- K. W. Lam, R. Uddin, C. Y. Liew, C. L. Tham, D. A. Israf, A. Syahida, M. B. A. Rahman, Z. Ul-Haq, and N. H. Lajis, *Med. Chem. Res.*, 2012, **21**, 1953-1966.
- J. Rojas, J. N. Dominguez, J. E. Charris, G. Lobo, M. Paya, and M. L. Ferrandiz, *Eur. J. Med. Chem.*, 2002, **37**, 699-705.
- J. V. Duncia, J. B. Santella, C. A. Higley, W. J. Pitts, J. Wityak, W. E. Frieze, F. W. Rankin, J. H. Sun, R. A. Earl, A. C. Tabaka, C. A. Teleha, K. F. Blom, M. F. Favata, E. J. Manos, A. J. Daulerio, D. A. Stradley, K. Horiuchi, R. A. Copeland, P. A. Scherle, J. M. Trzaskos, R. L. Magolda, G. L. Trainor, R. R. Wexler, F. W. Hobbs, and R. E. Olson, *Bioorg. Med. Chem. Lett.*, 1998, **8**, 2839-2844.
- F. Manna, F. Chimenti, A. Bolasco, A. Filippelli, A. Palla, W. Filippelli, E. Lampa, and R. Mercantini, *Eur. J. Med. Chem.*, 1992, **27**, 627-632.
- S. A. Cooke, G. K. Corlett, and A. C. Legon, *J. Chem. Soc. Faraday Transactions.*, 1998, **94**, 1565-1570.
- X. Qiu, Y. Du, B. Lou, Y. Zuo, W. Shao, Y. Huo, J. Huang, Y. Yu, B. Zhou, J. Du, H. Fu, and X. Bu, *J. Med. Chem.*, 2011, **53**, 8260-8273.
- G. L. Patrick, in *An Introduction to Medicinal Chemistry*. Oxford University Press, Oxford, 4th edn., 2009, ch 14, pp. 250.
- C. X. Xue, S. Y. Cui, M. C. Liu, Z. D. Hu, and B. T. Fan, *Eur. J. Med. Chem.*, 2004, **39**, 745-753.
- C. A. Lipinski, F. Lombardo, B. W. Dominy, and P. J. Feeney, *Adv. Drug Deliv. Rev.*, 2001, **46**, 3-26.
- E. H. Kerns, and L. Di, In *Drug-like Properties: Concepts, Structure Design and Methods*, Academic Press, San Diego, 2008, pp 122-136.
- E. H. Kerns, and L. Di, In *Drug-like Properties: Concepts, Structure Design and Methods*, Academic Press, San Diego, 2008, pp 197-208.
- E. H. Kerns, and L. Di, In *Drug-like Properties: Concepts, Structure Design and Methods*, Academic Press, San Diego, 2008, pp 215-223.
- D. Batovska, S. Parushev, A. Slavova, V. Bankova, I. Tsvetkova, M. Ninova, and H. Najdenski, *Eur. J. Med. Chem.*, 2007, **42**, 87-92.
- H. Jin, L. Xiang, F. Wen, K. Tao, Q. Liu, and T. Hou, *Tetrahedron. Sonochem.*, 2008, **15**, 681-683.
- J. F. McOmie, M. Watts, and D. E. West, *Tetrahedron.*, 1968, **24**, 2289-2292.